


# Icelike Vibrational Properties of Strong Hydrogen Bonds in Hydrated Lithium Nitrate

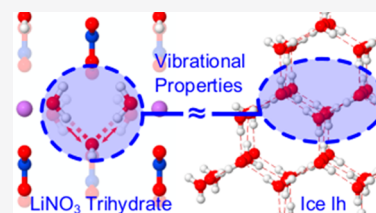
Daniel Hutzler, Klara Stallhofer, Reinhard Kienberger, Eberhard Riedle, and Hristo Iglev\*

 Cite This: *J. Phys. Chem. A* 2020, 124, 5784–5789 Read Online

ACCESS |

 Metrics & More Article Recommendations

**ABSTRACT:** The hydrogen bond network accounts for many of the extraordinary physical properties of liquid water and ice. Its vibrational dynamics are quite complex in their entirety but can be accessed in detail by investigating small groups of only a few water molecules. Here, aqueous salt hydrates turned out to be an exceptional model system for water molecules arranged in well-defined geometrical structures that can be accessed by means of femtosecond spectroscopy of the OH stretching vibration. In this study, we find striking resemblance between the vibrational properties of three water molecules connected via strong hydrogen bonds in the trihydrate of  $\text{LiNO}_3$  and those of ordinary ice  $\text{I}_h$ . As in ice, the vibrations of the hydrate water molecules show ultrafast excited state dynamics that are strongly accelerated when proceeding from deuterated to neat  $\text{H}_2\text{O}$  samples. The latter is analyzed by means of an additional relaxation channel that is due to Fermi resonance between the OH stretching vibration and the bend overtone accompanied by delocalization of the vibration over neighboring water molecules in the  $\text{H}_2\text{O}$  species. Moreover, in the hydrate and ice samples severe spectral broadening is examined when comparing fundamental and excited state absorption bands. Here, proton delocalization along the strong hydrogen bonds is given as a possible underlying mechanism.



## INTRODUCTION

Properties of ice, water, and any aqueous system are to a large extent determined by its hydrogen bond (H-bond) network. In liquid water, the H-bonded network fluctuates between icelike bonds and waterlike bonds.<sup>1,2</sup> Various studies suggest that the relative concentration and size of the associated substructures play a crucial role in aqueous systems, for example, in the density anomaly of water<sup>3–5</sup> or solvation of proteins.<sup>6</sup> The features of this dynamic network can be accessed via infrared vibrational spectroscopy. Here, the OH stretching vibration, which is very sensitive to its chemical vicinity, serves as an indicator for the vibrational characteristics of the investigated system.<sup>7–10</sup> However, it is very complicated to link spectral to structural features. This can be remedied by using the hydrates of inorganic salts that are an ideal model system for water molecules embedded in well-defined crystal matrices.<sup>11,12</sup> While the geometry of many of the local H-bonded substructures present in water can be reproduced in these models, they lack the dynamic breaking and reformation of H-bonds that is an essential characteristic of liquid water<sup>13</sup> and sets it apart from the static structure of the H-bond network in ice. The latter is dominated by strong and straight hydrogen bonds.<sup>14,15</sup>

In  $\text{LiNO}_3$  trihydrate, groups of three water molecules are enclosed within the crystal lattice. The water clusters comprise three types of H-bonds—weak, bifurcated, and strong bonds—that represent the major bonding motifs in liquid water and ice.<sup>16</sup> Here, we focus on the two strong and straight H-bonds along the OH–O direction with a length (O–O distance) of

282 pm. With these characteristics, they define a structural motif that is comparable with bulk ice, where the bond length lies at 275 pm.<sup>14,15</sup> Measurements on  $\text{LiNO}_3 \cdot (\text{HDO} + 2\text{D}_2\text{O})$  suggested similar vibrational relaxation for the OD stretching mode as in isotope-diluted ice, involving the bending mode and librations of the water molecule.<sup>17</sup> This emphasizes that hydrates indeed constitute suitable model systems for the vibrational relaxation dynamics of ice since the surrounding crystal matrix of the hydrate does not fundamentally alter the relaxation process.

To unravel the complex relaxation mechanisms of the OH stretching vibration in aqueous systems, it can help to compare samples that are prepared with neat  $\text{H}_2\text{O}$  to deuterated samples. This is because in the isotope-diluted samples resonant energy relaxation is barred due to the decoupling of the OD and OH vibrations. Hence, the resonant relaxation pathways that are exclusively present in pure  $\text{H}_2\text{O}$  samples can be derived from a comparison to the respective deuterated species.

In this study, we find that the stretching vibration of OH oscillators engaged in a strong “icelike” H-bond in a three-

Received: February 24, 2020

Revised: June 22, 2020

Published: June 23, 2020



membered cluster of water molecules in the trihydrate of  $\text{LiNO}_3$  exhibits relaxation characteristics which are unusual for water clusters in hydrated salts but indeed closely resemble the properties of ordinary ice  $\text{I}_h$ . In particular, we observe ultrafast vibrational relaxation dynamics, which accelerate significantly upon going from deuterated to neat  $\text{H}_2\text{O}$  samples. Moreover, in the hydrate, as well as in ice samples, severe spectral broadening is observed when proceeding from the fundamental to the excited state absorption (ESA). Based on the findings for ice, we suggest that a Fermi resonance between the OH bending overtone and the OH stretching vibration, as well as proton delocalization along the strong H-bond, is a key factor influencing the unusual vibrational properties of  $\text{LiNO}_3$  trihydrate.

## EXPERIMENTAL METHODS

**Infrared Absorption Spectroscopy.** Steady state absorption spectra are conducted with a commercial VECTOR 22 Fourier-transform infrared spectrometer (FTIR; Bruker Optics) that allows a spectral resolution of  $0.5 \text{ cm}^{-1}$ . The setup used to record the time-resolved data was previously described elsewhere.<sup>18,19</sup> In the following, only the relevant parameters are given. Mid-IR pump pulses are generated by optical parametric amplification (OPA) with preamplification in the visible spectral range. The system is pumped by  $300 \mu\text{J}$  pulses at a center wavelength of  $778 \text{ nm}$  (CPA 2010; Clark MXR). In this way, mid-IR pulses with energies on the microjoule level are produced. The probe pulses are generated in a one-stage OPA pumped by  $100 \mu\text{J}$  yielding extremely broadband pulses of spectral widths up to  $1 \mu\text{m}$  and energies of several hundred nanojoules. Pump and probe pulses are close to the Fourier limit with durations of roughly  $50 \text{ fs}$ . The polarizations of pump and probe are kept parallel throughout this study. The pump bandwidth can be controlled by a  $4f$  grating spectral selector. In our measurements, pump pulses of appropriate full width at half-maximum (fwhm) were tuned to the fundamental absorption bands of the OH oscillators under investigation. Specifically, the ice samples ( $\text{H}_2\text{O}$  and  $\text{HDO:D}_2\text{O}$ ) were excited at a frequency of  $3300 \text{ cm}^{-1}$  with a fwhm of  $\sim 200 \text{ cm}^{-1}$ , while the hydrates were excited around  $3400 \text{ cm}^{-1}$  with a fwhm of  $\sim 100 \text{ cm}^{-1}$ . The broadband probe pulses have a typical fwhm of about  $400 \text{ cm}^{-1}$ . For more details on the experimental setup, see Bradler et al.<sup>18</sup>

After passing the sample, the probe beam is spectrally resolved in a polychromator and subsequently recorded on a multichannel IR detection system. The transient data are monitored in the change of the optical density  $\Delta\text{OD} = -\log(T/T_0)$  with  $T$  the probe transmission through an excited sample and  $T_0$  the transmission through an unexcited sample, i.e., with the pump beam blocked. To analyze the time-resolved measurements, an exponential decay is fitted to the data. The exponential is convoluted with a Gaussian accounting for the instrument response function. Considering the spectral widths of the used pump and probe pulses, mentioned just above, the latter amounts to  $90 \text{ fs}$  for the ice measurements and to  $145 \text{ fs}$  for the respective measurements in the hydrate samples. Note that coherent effects can occur on time scales shorter than the instrument response. For the given time constants of vibrational relaxation, several measurements on separately prepared samples are taken into account.

**Sample Preparation.** The deuterated solvents are prepared by isotopic exchange in a mixture of appropriate amounts of  $\text{H}_2\text{O}$  and  $\text{D}_2\text{O}$ . All hydrate samples are close to the

saturation limit of the  $\text{LiNO}_3$  salt (99.9%, Aldrich). The crystalline samples are obtained by slowly cooling the respective solution between two  $\text{CaF}_2$  windows in an evacuated sample chamber.

## RESULTS AND DISCUSSION

**Spectral and Dynamical Properties of  $\text{LiNO}_3$  Trihydrate.** The crystal structure of  $\text{LiNO}_3$  trihydrate is known from X-ray and neutron diffraction studies.<sup>20,21</sup> It is depicted in Figure 1a. The hydrate water molecules form three different

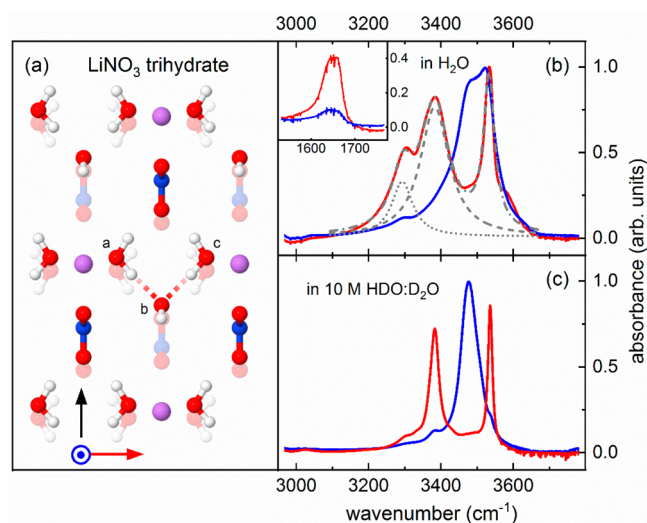


**Figure 1.** Crystal structure and steady state absorption of  $\text{LiNO}_3$  trihydrate. (a) Crystal structure of  $\text{LiNO}_3$  trihydrate (H in white, Li in violet, N in blue, and O in red). The black arrow marks the propagation direction of the laser light. (b) Normalized FTIR spectra of  $\text{LiNO}_3 \cdot 3\text{H}_2\text{O}$ . Red and blue spectra are recorded applying perpendicular polarizations, as marked by the colored arrows in (a). Shown in gray is a cumulative fit with three Lorentz peaks (dash-dotted line) and the individual peaks representing the OH bending overtone (dotted line) and the strong OH stretching vibration (dashed line). The inset shows the  $\text{H}_2\text{O}$  bending mode. (c) Respective spectra of  $\text{LiNO}_3 \cdot (\text{HDO} + 2\text{D}_2\text{O})$ . All measurements were conducted at a sample temperature of  $220 \text{ K}$ .

types of H bonds, which are found in two perpendicular planes. A strong H-bond is developed between the water molecules a and b and the molecules c and b, respectively (dashed lines in Figure 1a). With respect to their length, geometry, and strength, these straight bonds are very similar to the ones found for bulk ice. Thereby, a structural motif comprising two icelike H-bonds is formed from the three water molecules. In the same plane, a rather weak bond is found between the second OH group of molecule a (or c) and the nearest oxygen atom of the neighboring nitrate anion. The third type of bond lies in a plane normal to the figure plane. It is a bifurcated bond of medium energy that forms between each of the OH groups of water molecule b and two oxygen atoms of a nearby  $\text{NO}_3^-$  ion.

When the crystal is properly oriented with respect to the propagation direction of the excitation light, the correct polarization yields exclusive excitation of the OH groups involved in the weak and strong H-bonds. Rotating the polarization by  $90^\circ$  then solely addresses the oscillators associated with the bifurcated bonds. This applies to laser light traversing along the direction indicated by the black arrow

in Figure 1a. Corresponding polarization-resolved FTIR spectra of  $\text{LiNO}_3$  dissolved in  $\text{H}_2\text{O}$  and 10 M  $\text{HDO}:\text{D}_2\text{O}$  at 220 K are given in Figures 1b and 1c. Both figures show two separate spectra recorded with perpendicular polarizations.

The vibrational properties of the  $\text{LiNO}_3 \cdot (\text{HDO} + 2\text{D}_2\text{O})$  sample were previously described elsewhere<sup>16,18</sup> and are shortly summarized here. In Figure 1c, the two peaks of the red curve are situated at 3383 and 3536  $\text{cm}^{-1}$  and exhibit fwhm's of 31 and 14  $\text{cm}^{-1}$  (Lorentz fits). They pertain to the OH groups engaged in the strong and weak H-bonds. A small shoulder in the low-energy flank of the peak due to the strong H bonds around 3300  $\text{cm}^{-1}$  most probably is due to a small contamination with  $\text{H}_2\text{O}$  molecules. The absorption at 3475  $\text{cm}^{-1}$  in the blue-colored spectrum of Figure 1c stems from the OH groups involved in the bifurcated H-bond. Previous studies showed that the band is inhomogeneously broadened, which was investigated with regard to the coupling to a low-lying wagging mode.<sup>16</sup> Small shoulders occur in the high- and low-energy wings at the spectral positions of the OH stretching vibrations of the strong and weak H-bonds. A polarization direction not perfectly matching the crystal orientation as well as slight polycrystallinity of the sample could both account for these features.

For the spectra of  $\text{LiNO}_3 \cdot 3\text{H}_2\text{O}$  shown in Figure 1b, the assignment of the individual peaks is more demanding. Comparison of the red curve with the corresponding one for the isotope-diluted hydrate in Figure 1c indicates that the peaks at 3385 and 3532  $\text{cm}^{-1}$  with fwhm's of 97 and 38  $\text{cm}^{-1}$  are due to the strong and weak H-bonds. The spectral positions and widths are determined from a cumulative fit of three Lorentz peaks as shown in Figure 1b. Note that there is no splitting into symmetric and antisymmetric stretching vibrations: Since the two features pertain to two OH groups of the same water molecule, their mutual energy distance of about 150  $\text{cm}^{-1}$  hinders resonance, thus decoupling the two OH groups. This explains the good energy match with the HDO bands. The third absorption at 3293  $\text{cm}^{-1}$ , however, is new to the spectrum. Its frequency matches well with twice the frequency of the  $\text{H}_2\text{O}$  bending mode at 1650  $\text{cm}^{-1}$  (inset in Figure 1b). Thus, we ascribe the feature to the bend overtone. The inset in Figure 1b shows that the bending fundamental only has a considerable amplitude for excitation with polarization in the plane of the figure (red curve). This is because the bending mode's dipole moment coincides with the propagation direction of the incident laser light for molecule b. Considering molecules a and c, it is striking that the amplitudes of the bending overtone and fundamental are very similar (red curves), given that overtone transitions are usually weak compared to the respective fundamental absorption. This points toward an enhancement of the bend overtone which can be explained by invoking a Fermi resonance between the bend overtone and the close-lying hydrate peak of the strongly H-bonded OH groups at 3385  $\text{cm}^{-1}$ .<sup>22</sup> Associated resonance broadening would also explain the wider spectrum of the strong hydrate peak in the pure  $\text{H}_2\text{O}$  sample as compared to the deuterated one. Furthermore, considerable intermolecular coupling can lead to delocalization of the stretching vibration on the water trimer, in particular on the molecules a and c. Similar to the formation of vibrational excitons in neat ice,<sup>23,24</sup> this delocalization can significantly modify the shape of the strong and weak OH stretching bands. Another small shoulder around 3575  $\text{cm}^{-1}$  occurs in the high-energy wing of the OH stretching peak corresponding to the weak H-bond. In

previous studies on  $\text{HDO}:\text{D}_2\text{O}$  ice, a similar band was ascribed to a combination band of the OH stretching vibration and a low-frequency lattice mode.<sup>23,25</sup>

Lastly, the blue curve represents absorption by the water molecules involved in the bifurcated H-bond. It is centered at 3500  $\text{cm}^{-1}$  and is subdivided into two features with an energy distance of about 50  $\text{cm}^{-1}$ . The splitting of this band is not due to symmetric and asymmetric stretching: The symmetric vibration cannot be accessed because of its dipole moment being collinear to the propagation direction of the incident laser light. It is more likely that the split up is evoked by coupling to low-lying intermolecular vibrations. In particular, a wagging mode of the water molecules, which has recently been discussed, is considered.<sup>16</sup>

Turning to the dynamic vibrational properties of  $\text{LiNO}_3$  trihydrate, Figure 2a shows a pump–probe transient measured

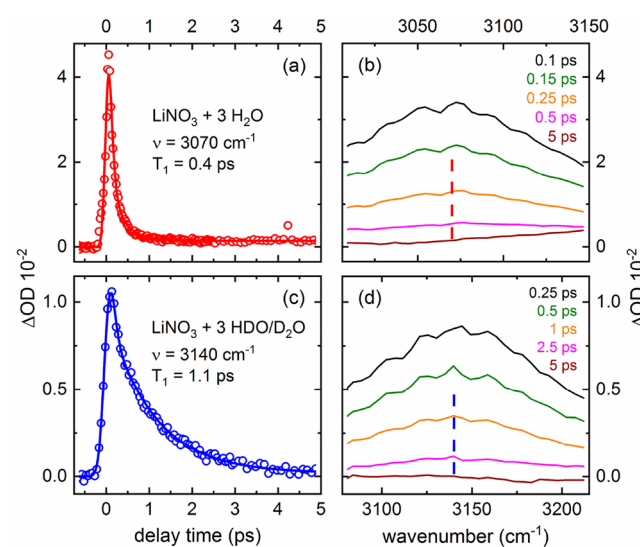


**Figure 2.** Transient absorption measurements on  $\text{LiNO}_3$  trihydrate. All measurements were conducted at a sample temperature of 220 K after excitation of the OH stretching vibration that is associated with the strong hydrogen bond at  $\sim 3400 \text{ cm}^{-1}$ . (a) Pump–probe transient measured in the ESA of  $\text{LiNO}_3 \cdot 3\text{H}_2\text{O}$  at 3070  $\text{cm}^{-1}$ . (b) Corresponding transient spectra measured at different ESA delay times after pump excitation. (c) Transient measured in the ESA of  $\text{LiNO}_3 \cdot (\text{HDO} + 2\text{D}_2\text{O})$  at 3140  $\text{cm}^{-1}$ . (d) Related transient spectra recorded at different delays. The dashed lines in (b) and (d) indicate the spectral positions of the associated transients in (a) and (c).

at a sample temperature of 220 K upon excitation in the fundamental absorption band around 3400  $\text{cm}^{-1}$ . The data are recorded at a frequency of 3070  $\text{cm}^{-1}$ , where the ESA representing the OH stretching related to the strong H-bond in the  $\text{H}_2\text{O}$  sample reaches its maximum. The OH stretching decay time is determined to be  $(0.40 \pm 0.05) \text{ ps}$ . Respective transient spectra can be seen in Figure 2b and show that the vibrational dynamics are not frequency dependent. Small absorption changes in the high-energy end at a delay of 5 ps are assigned to laser-induced transient heating of the sample.<sup>8</sup> Corresponding data for the deuterated sample are shown in Figure 2c and 2d. Here, a population decay time of  $(1.1 \pm 0.1) \text{ ps}$  is extracted in the maximum of the ESA at 3140  $\text{cm}^{-1}$  in good agreement with previous measurements.<sup>16,18</sup> With a fwhm of  $\sim 125 \text{ cm}^{-1}$ , as determined in these preceding studies covering a wider spectral range including the ground state bleaching, the absorption in the excited state of  $\text{LiNO}_3 \cdot (\text{HDO}$



+ 2D<sub>2</sub>O) is about four times broader than the fundamental absorption band, with a fwhm of 30 cm<sup>-1</sup>, as found above. As far as can be judged from the narrower spectral range covered in Figure 2d, the broadening observed in this measurement might even be more pronounced.

The vibrational lifetimes in the deuterated and the H<sub>2</sub>O LiNO<sub>3</sub> trihydrate are exceptionally short compared to H-bond dynamics observed for other hydrated salts. Our previous measurements on the weakly H-bonded water molecules in deuterated NaClO<sub>4</sub> monohydrate and NaCl dihydrate gave evidence of lifetimes of 7.2<sup>12</sup> and 6.8 ps,<sup>11</sup> respectively. In Ba(ClO<sub>4</sub>)<sub>2</sub>·3H<sub>2</sub>O that also features a cluster of three water molecules, yet lacks H-bonding between them, a time constant of 8 ps is found.<sup>26</sup> Moreover, the data indicate only little or no spectral broadening in the ESA in these cases. While the vibrational properties of the strong H-bonds in LiNO<sub>3</sub> trihydrate—namely substantial broadening of the ESA and extremely fast vibrational relaxation—thus stand out markedly among those of water clusters within hydrated salts, they are indeed comparable to the characteristics of ice, as shown in the following.

**Comparison between the Vibrational Properties of LiNO<sub>3</sub> Trihydrate and Ice.** Figure 3a depicts the absorption

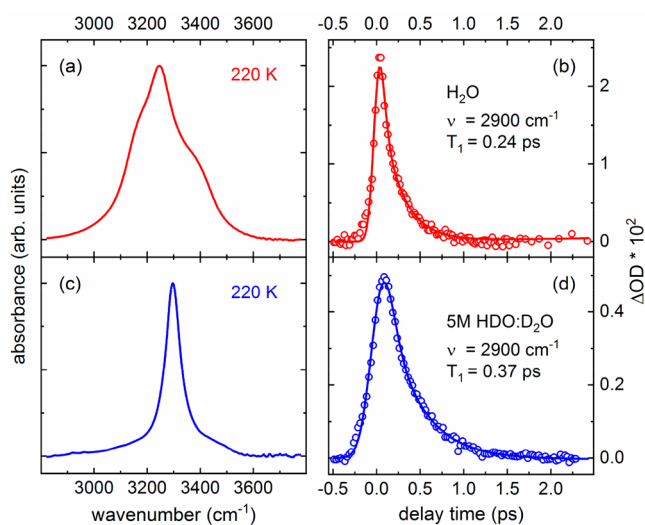


**Figure 3.** Steady state absorption and vibrational dynamics of ice I<sub>h</sub>. All measurements were performed at a sample temperature of 220 K. The time-resolved data were conducted after pump excitation at ~3300 cm<sup>-1</sup>. (a) Normalized FTIR spectra of the OH stretching region in H<sub>2</sub>O ice. (b) Pump–probe transient (circles) and fit (solid line) measured in the ESA of H<sub>2</sub>O ice at 2900 cm<sup>-1</sup>. (c) OH stretch region of 5 M HDO:D<sub>2</sub>O in the solid phase (red). (d) Pump–probe transient and fit recorded in the ESA of 5 M HDO:D<sub>2</sub>O at 2900 cm<sup>-1</sup>.

spectrum of H<sub>2</sub>O ice I<sub>h</sub> in the OH stretching region. It shows the well-known broad absorption band centered around 3250 cm<sup>-1</sup>, whose particular substructure is still subject to discussion. Besides the splitting into symmetric and asymmetric stretching vibrations, several factors are believed to contribute to the band's shape. These include coupling to low-frequency intermolecular modes<sup>9,27</sup> and delocalized intermolecular vibrations (vibrational excitons) that form when the excited OH stretch transition dipoles add up as a consequence of strong intra- and intermolecular coupling.<sup>23,24</sup> Another significant factor is the enhancement of the bend overtone by Fermi resonance with the OH stretching vibration.<sup>28,29</sup> It has

been shown by Skinner and co-workers that it is necessary to account for the influence of the Fermi resonance in order to reproduce the lower energy side of the ice spectrum to a satisfactory degree.<sup>22</sup>

The respective spectrum of an isotopically diluted sample consisting of 5 M HDO in D<sub>2</sub>O is given in Figure 3c. The stretching band is much narrower than the one of the neat ice sample. It features a fwhm of only 70 cm<sup>-1</sup> centered around 3295 cm<sup>-1</sup>. The bend overtone of HDO is centered around 2950 cm<sup>-1</sup>,<sup>30</sup> well below the stretching vibration, and thus is not expected to have an influence on the spectrum of the latter.

The transition from the first to the second vibrational level in neat ice is known to be very flat and broad.<sup>9,31</sup> Since a diverse range of processes influences the spectral shape already in the ground state of H<sub>2</sub>O ice, as noted above, we focus on the deuterated ice in the following discussion. Comparing the bandwidth in the excited state to the ground state absorption, broadening by a factor of about 5 (230 K)<sup>32</sup>–6 (180 K)<sup>33</sup> has been reported in samples of lower isotope dilution. Such broadening has been ascribed to the quantum mechanical delocalization of the vibrational wave function along the O–O direction of the hydrogen bond. This proton delocalization in the vibrationally excited state results in a wide range of effective O–O distances and thereby gives rise to Franck–Condon-like transitions over a broad frequency range.<sup>34</sup> In LiNO<sub>3</sub> trihydrate, the strong icelike hydrogen bonds would likewise facilitate such delocalization that could account for the observed broadening of the ESA, which is more than four times wider than the ground state absorption.

Figures 3b and 3d show pump–probe data measured in the ESAs of HDO and H<sub>2</sub>O ice at a frequency of 2900 cm<sup>-1</sup> and a sample temperature of 220 K upon pumping the ground state absorption around 3300 cm<sup>-1</sup>. The measurements yield ultrafast vibrational lifetimes  $T_1$  of (0.24 ± 0.05) and (0.37 ± 0.05) ps for the neat and deuterated ice samples, respectively. For the spectral range under observation, the vibrational lifetimes show no dependence on frequency. These values are in good agreement with the ones found in the literature<sup>10,35,36</sup> and give evidence of distinctly accelerated dynamics in the neat H<sub>2</sub>O sample. A possible explanation for this acceleration can be found in the aforementioned Fermi resonance between the OH stretching vibration and the bend overtone in H<sub>2</sub>O ice, which is lacking in the deuterated sample. In addition, delocalization of the stretching vibration over several water molecules can further accelerate vibrational relaxation. This mechanism is also hindered in deuterated samples, since in a 5 M solution of HDO in D<sub>2</sub>O on average only every 11th molecule contains an OH group, impeding resonant energy transfer between OH oscillators. Note that potential vibrational relaxation via Fermi resonance or vibrational delocalization, respectively, opens up an additional relaxation pathway in the H<sub>2</sub>O sample and results in a reduction of the vibrational lifetime by ~1/3. In a simplified physical picture, we represent this relaxation channel by a corresponding relaxation rate. Being only present in H<sub>2</sub>O samples, this rate can be extracted from the difference of the effective relaxation rates of the H<sub>2</sub>O and deuterated samples, which results in  $k_{ice} = (1/T_1)_{H_2O} - (1/T_1)_{HDO} \sim 1.5 \text{ ps}^{-1}$ .

Significant acceleration is also observed in LiNO<sub>3</sub> trihydrate when going from HDO to H<sub>2</sub>O as solvent. The additional relaxation rate of  $k_{LiNO_3} = (1/T_1)_{LiNO_3 \cdot H_2O} - (1/T_1)_{LiNO_3 \cdot HDO} \sim 1.6 \text{ ps}^{-1}$  is, in fact, comparable to the one obtained for ice. The good agreement between these relaxation rates hints at a

common underlying process leading to the accelerated decay for the H<sub>2</sub>O samples of both LiNO<sub>3</sub> trihydrate and ice.

In light of the prominent spectral contribution of the bend overtone in the H<sub>2</sub>O hydrate sample and the lack of overlap between bend overtone and stretching vibration in the deuterated case, Fermi resonance is likely to be a key factor in the acceleration observed in the hydrate, paralleling the discussion for ice. While Fermi resonance is in itself an intramolecular process, the necessary spectral overlap between the OH stretching vibration and the bending overtone is only attained in the presence of strong OH bonding, as is the case for the three-membered water clusters in LiNO<sub>3</sub> trihydrate. In other hydrates, such as NaClO<sub>4</sub> containing only isolated water molecules<sup>12</sup> or Ba(ClO<sub>4</sub>)<sub>2</sub>·3H<sub>2</sub>O with a cluster of three molecules lacking H-bonding,<sup>26</sup> no such effect and associated acceleration are observed. Thus, the specific geometric arrangement of the water molecules within the cluster and the resulting strong H-bonds are indeed a prerequisite for the development of resonance conditions and “icelike” dynamics. Delocalization of the stretching vibration over the water trimer in LiNO<sub>3</sub>·3H<sub>2</sub>O, in particular the resonant coupling between molecules a and c in Figure 1a, on the other hand, can also contribute to the acceleration of the vibrational relaxation. In water and ice, calculations indicate delocalization over up to 12 OH groups<sup>37,38</sup> and even to the whole crystal,<sup>39</sup> respectively. The influence of vibrational delocalization is also supported by experimental evidence.<sup>40</sup> Due to the crystal structure of the trihydrate, however, delocalization is limited to the three water molecules a, b, and c of one cluster (see Figure 1a). In combination with the similarity of the relaxation rates  $k_{\text{ice}}$  and  $k_{\text{LiNO}_3}$ , this suggests either that the impact of vibrational delocalization in the relaxation of H<sub>2</sub>O ice is dominated by delocalization over the closest neighboring water molecules, as well, or that the effect does generally play a secondary role in the relaxation of both the ice and the trihydrate samples. The latter conclusion would once more emphasize the essential role of Fermi resonance in the vibrational relaxation process of H<sub>2</sub>O samples.

The “smallest drop of water” often is referred to as the smallest water cluster in which the monomers form a fully three-dimensional hydrogen-bonded (H-bonded) network.<sup>41–43</sup> For ice, the cluster with the smallest number of molecules still showing crystallization in hexagonal structure, according to infrared spectra, has been identified as the cyclic water hexamer.<sup>44,45</sup> In both cases, the minimum number of molecules involved amounts to six. In this study, we show that with regard to vibrational properties three strongly bound water molecules in the trihydrate of LiNO<sub>3</sub> already suffice to emulate key features of the OH stretching of ordinary ice.

## CONCLUSION

In summary, we find a striking resemblance between the vibrational properties of the strong H-bonds within a three-membered motif of water molecules in LiNO<sub>3</sub> trihydrate and ice. Both samples exhibit ultrafast relaxation dynamics of the OH stretching vibration. Moreover, significant broadening of the ESA is observed in the deuterated ice and trihydrate samples, reaching a width of several times that of the ground state absorption. As discussed above, this may be due to the delocalization of the vibrational wave function (or proton delocalization) along the strong hydrogen bond. When comparing the vibrational lifetimes of the isotope diluted to those of the H<sub>2</sub>O samples, strongly decelerated relaxation

dynamics are observed in the deuterated ice and hydrate species. Fermi resonance between the OH stretching vibration and the bend overtone, in combination with the delocalization of the stretching vibration over the closest neighboring water molecules, appears to be the dominant process yielding accelerated dynamics in neat H<sub>2</sub>O samples. Both mechanisms can be interpreted as an additional relaxation channel present in the undeuterated samples. With a respective relaxation rate on the order of 1.5 ps<sup>-1</sup>, the rates are very similar in ice and in the trihydrate.

Altogether, our study shows that the three water molecules a, b, and c in Figure 1a reproduce key spectral and dynamical properties of the OH stretching in ordinary ice I<sub>h</sub>. As far as dynamic vibrational properties are concerned, one can thus say that the “smallest ice crystal”—as found in LiNO<sub>3</sub> trihydrate—consists of not more than three water molecules.

## AUTHOR INFORMATION

### Corresponding Author

Hristo Iglev – Physik-Department E11, Technische Universität München, 85748 Garching, Germany; [orcid.org/0000-0001-9208-0068](https://orcid.org/0000-0001-9208-0068); Email: [Hristo.Iglev@ph.tum.de](mailto:Hristo.Iglev@ph.tum.de)

### Authors

Daniel Hutzler – Physik-Department E11, Technische Universität München, 85748 Garching, Germany

Klara Stallhofer – Physik-Department E11, Technische Universität München, 85748 Garching, Germany; [orcid.org/0000-0001-6314-0156](https://orcid.org/0000-0001-6314-0156)

Reinhard Kienberger – Physik-Department E11, Technische Universität München, 85748 Garching, Germany

Eberhard Riedle – Lehrstuhl für BioMolekulare Optik, Ludwig-Maximilians-Universität München, 80538 München, Germany; [orcid.org/0000-0002-2672-5718](https://orcid.org/0000-0002-2672-5718)

Complete contact information is available at: <https://pubs.acs.org/10.1021/acs.jpca.0c01588>

### Notes

The authors declare no competing financial interest.

## ACKNOWLEDGMENTS

We acknowledge the Deutsche Forschungsgemeinschaft for the financial support via the German Excellence Strategy (Munich-Centre of Advanced Photonics (MAP)) and the European Research Council via Consolidator Grant AEDMOS (Grant Nr. 647695).

## REFERENCES

- (1) Laenen, R.; Rauscher, C.; Laubereau, A. Dynamics of local substructures in water observed by ultrafast infrared hole burning. *Phys. Rev. Lett.* **1998**, *80*, 2622–2625.
- (2) Overduin, S. D.; Patey, G. N. Fluctuations and local ice structure in model supercooled water. *J. Chem. Phys.* **2015**, *143*, 094504.
- (3) Errington, J. R.; Debenedetti, P. G.; Torquato, S. Cooperative origin of low-density domains in liquid water. *Phys. Rev. Lett.* **2002**, *89*, 215503.
- (4) Matsumoto, M. Why does water expand when it cools? *Phys. Rev. Lett.* **2009**, *103*, 17801.
- (5) Sedlmeier, F.; Horinek, D.; Netz, R. R. Spatial correlations of density and structural fluctuations in liquid water: a comparative simulation study. *J. Am. Chem. Soc.* **2011**, *133*, 1391–1398.
- (6) Meister, K.; Strazdaite, S.; DeVries, A. L.; Lotze, S.; Olijve, L. L. C.; Voets, I. K.; Bakker, H. J. Observation of ice-like water layers at an

aqueous protein surface. *Proc. Natl. Acad. Sci. U. S. A.* **2014**, *111*, 17732–17736.

(7) Perakis, F.; de Marco, L.; Shalit, A.; Tang, F.; Kann, Z. R.; Kühne, T. D.; Torre, R.; Bonn, M.; Nagata, Y. Vibrational spectroscopy and dynamics of water. *Chem. Rev.* **2016**, *116*, 7590–7607.

(8) Iglev, H.; Schmeisser, M.; Simeonidis, K.; Thaller, A.; Laubereau, A. Ultrafast superheating and melting of bulk ice. *Nature* **2006**, *439*, 183–186.

(9) Perakis, F.; Hamm, P. Two-dimensional infrared spectroscopy of neat ice Ih. *Phys. Chem. Chem. Phys.* **2012**, *14*, 6250–6256.

(10) Woutersen, S.; Emmerichs, U.; Nienhuys, H.-K.; Bakker, H. Anomalous temperature dependence of vibrational lifetimes in water and ice. *Phys. Rev. Lett.* **1998**, *81*, 1106–1109.

(11) Pandelov, S.; Pilles, B. M.; Werhahn, J. C.; Iglev, H. Time-resolved dynamics of the OH stretching vibration in aqueous NaCl hydrate. *J. Phys. Chem. A* **2009**, *113*, 10184–10188.

(12) Hutzler, D.; Werhahn, J. C.; Heider, R.; Bradler, M.; Kienberger, R.; Riedle, E.; Iglev, H. Highly selective relaxation of the OH stretching overtones in isolated HDO molecules observed by infrared pump-repump-probe spectroscopy. *J. Phys. Chem. A* **2015**, *119*, 6831–6836.

(13) Nibbering, E. T. J.; Elsaesser, T. Ultrafast vibrational dynamics of hydrogen bonds in the condensed phase. *Chem. Rev.* **2004**, *104*, 1887–1914.

(14) Kuhs, W. F.; Lehmann, M. S. The structure of the ice Ih by neutron diffraction. *J. Phys. Chem.* **1983**, *87*, 4312–4313.

(15) Bergmann, U.; Di Cicco, A.; Wernet, P.; Principi, E.; Glatzel, P.; Nilsson, A. Nearest-neighbor oxygen distances in liquid water and ice observed by X-ray Raman based extended X-ray absorption fine structure. *J. Chem. Phys.* **2007**, *127*, 174504.

(16) Werhahn, J. C.; Pandelov, S.; Xantheas, S. S.; Iglev, H. Dynamics of weak, bifurcated, and strong hydrogen bonds in lithium nitrate trihydrate. *J. Phys. Chem. Lett.* **2011**, *2*, 1633–1638.

(17) Smit, W. J.; Bakker, H. J. Vibrational energy relaxation of water molecules in a hydrated lithium nitrate crystal. *J. Phys. Chem. C* **2016**, *120*, 11078–11084.

(18) Bradler, M.; Werhahn, J. C.; Hutzler, D.; Fuhrmann, S.; Heider, R.; Riedle, E.; Iglev, H.; Kienberger, R. A novel setup for femtosecond pump-repump-probe IR spectroscopy with few cycle CEP stable pulses. *Opt. Express* **2013**, *21*, 20145–20158.

(19) Bradler, M.; Homann, C.; Riedle, E. Mid-IR femtosecond pulse generation on the microjoule level up to 5  $\mu\text{m}$  at high repetition rates. *Opt. Lett.* **2011**, *36*, 4212–4214.

(20) Hermansson, K.; Thomas, J. O.; Olovsson, I. Hydrogen bond studies. CXX. An X-Ray determination of the crystal structure of  $\text{LiNO}_3 \cdot 3\text{H}_2\text{O}$ . *Acta Crystallogr., Sect. B: Struct. Crystallogr. Cryst. Chem.* **1977**, *33*, 2857–2861.

(21) Hermansson, K.; Thomas, J. O.; Olovsson, I. Hydrogen bond Studies. CXXXVIII. Neutron diffraction studies of  $\text{LiNO}_3 \cdot 3\text{H}_2\text{O}$  at 120 and 295 K. *Acta Crystallogr., Sect. B: Struct. Crystallogr. Cryst. Chem.* **1980**, *36*, 1032–1040.

(22) Kananenka, A. A.; Skinner, J. L. Fermi resonance in OH-stretch vibrational spectroscopy of liquid water and the water hexamer. *J. Chem. Phys.* **2018**, *148*, 244107.

(23) Li, F.; Skinner, J. L. Infrared and Raman line shapes for Ice Ih. II.  $\text{H}_2\text{O}$  and  $\text{D}_2\text{O}$ . *J. Chem. Phys.* **2010**, *133*, 244504.

(24) Buch, V.; Devlin, J. P. A new interpretation of the OH-stretch spectrum of ice. *J. Chem. Phys.* **1999**, *110*, 3437–3443.

(25) Scherer, J. R.; Snyder, R. G. Raman intensities of single crystal ice Ih. *J. Chem. Phys.* **1977**, *67*, 4794–4811.

(26) Hutzler, D.; Brunner, C.; Petkov, P. S.; Heine, T.; Fischer, S. F.; Riedle, E.; Kienberger, R.; Iglev, H. Dynamics of the OH stretching mode in crystalline  $\text{Ba}(\text{ClO}_4)_2 \cdot 3\text{H}_2\text{O}$ . *J. Chem. Phys.* **2018**, *148*, 054307.

(27) Whalley, E. A detailed assignment of the O–H stretching bands of ice I. *Can. J. Chem.* **1977**, *55*, 3429–3441.

(28) Bergren, M. S.; Rice, S. A. An improved analysis of the OH stretching region of the vibrational spectrum of ice Ih. *J. Chem. Phys.* **1982**, *77*, 583–602.

(29) Rice, S. A.; Bergren, M. S.; Belch, A. C.; Nielsen, G. A theoretical analysis of the hydroxyl stretching spectra of ice Ih, liquid water, and amorphous solid water. *J. Phys. Chem.* **1983**, *87*, 4295–4308.

(30) de Marco, L.; Ramasesha, K.; Tokmakoff, A. Experimental evidence of Fermi resonances in isotopically dilute water from ultrafast broadband IR spectroscopy. *J. Phys. Chem. B* **2013**, *117*, 15319–15327.

(31) Shi, L.; Skinner, J. L.; Jansen, T. L. C. Two-dimensional infrared spectroscopy of neat ice Ih. *Phys. Chem. Chem. Phys.* **2016**, *18*, 3772–3779.

(32) Seifert, G.; Weidlich, K.; Graener, H. Picosecond ir hole-burning spectroscopy on HDO ice Ih. *Phys. Rev. B: Condens. Matter Mater. Phys.* **1997**, *56*, R14231–R14234.

(33) Dokter, A. M.; Bakker, H. J. Transient absorption of vibrationally excited ice Ih. *J. Chem. Phys.* **2008**, *128*, 024502.

(34) Perakis, F.; Widmer, S.; Hamm, P. Two-dimensional infrared spectroscopy of isotope-diluted ice Ih. *J. Chem. Phys.* **2011**, *134*, 204505.

(35) Timmer, R. L. A.; Bakker, H. J. Vibrational förster transfer in ice Ih. *J. Phys. Chem. A* **2010**, *114*, 4148–4155.

(36) Lock, A. J.; Bakker, H. J. Temperature dependence of vibrational relaxation in liquid  $\text{H}_2\text{O}$ . *J. Chem. Phys.* **2002**, *117*, 1708–1713.

(37) Auer, B. M.; Skinner, J. L. IR and Raman spectra of liquid water: theory and interpretation. *J. Chem. Phys.* **2008**, *128*, 224511.

(38) Auer, B. M.; Skinner, J. L. Vibrational sum-frequency spectroscopy of the water liquid/vapor interface. *J. Phys. Chem. B* **2009**, *113*, 4125–4130.

(39) Moberg, D. R.; Straight, S. C.; Knight, C.; Paesani, F. Molecular origin of the vibrational structure of ice Ih. *J. Phys. Chem. Lett.* **2017**, *8*, 2579–2583.

(40) Smit, W. J.; Versluis, J.; Backus, E. H. G.; Bonn, M.; Bakker, H. J. Reduced near-resonant vibrational coupling at the surfaces of liquid water and ice. *J. Phys. Chem. Lett.* **2018**, *9*, 1290–1294.

(41) Pérez, C.; Muckle, M. T.; Zaleski, D. P.; Seifert, N. A.; Temelso, B.; Shields, G. C.; Kisiel, Z.; Pate, B. H. Structures of cage, prism, and book isomers of water hexamer from broadband rotational spectroscopy. *Science* **2012**, *336*, 897–901.

(42) Wang, Y.; Babin, V.; Bowman, J. M.; Paesani, F. The water hexamer: cage, prism, or both. Full dimensional quantum simulations say both. *J. Am. Chem. Soc.* **2012**, *134*, 11116–11119.

(43) Liu, K.; Brown, M. G.; Carter, C.; Saykally, R. J.; Gregory, J. K.; Clary, D. C. Characterization of a cage form of the water hexamer. *Nature* **1996**, *381*, 501–503.

(44) Pradzynski, C. C.; Forck, R. M.; Zeuch, T.; Slaviček, P.; Buck, U. A fully size-resolved perspective on the crystallization of water clusters. *Science* **2012**, *337*, 1529–1532.

(45) Nauta, K.; Miller, R. E. Formation of cyclic water hexamer in liquid helium: the smallest piece of ice. *Science* **2000**, *287*, 293–295.